

Large Eddy Simulation of Near-Nozzle Shock Structure and Mixing Characteristics of Hydrogen Jets for Direct-Injection Spark-Ignition Engines

Hamzehloo A. and Aleiferis P.G.*

*Author for correspondence

Department of Mechanical Engineering,
 University College London (UCL),
 Torrington Place, London, WC1E 7JE,
 United Kingdom,
 E-mail: p.aleiferis@ucl.ac.uk

ABSTRACT

Due to the ever increasing prices of conventional fossil fuels, as well as climate change and sustainability issues, several liquids and gases have been proposed as alternative fuels for internal combustion engines. Hydrogen has been investigated by several researchers as a promising alternative gaseous fuel. In general gaseous fuels are injected either in the intake port of an internal combustion engine or directly into the cylinder. Direct injection of hydrogen offers higher volumetric efficiency and eliminates abnormal combustion phenomena like pre-ignition and backfire. However, due to hydrogen's low density, direct injection requires high injection pressures to achieve suitable mass flow rates for fast in-cylinder fuel delivery and mixing. Such pressures typically lead to choked conditions at the nozzle exit, followed by a turbulent under-expanded jet. Therefore, fundamental understanding of the expansion process and turbulent mixing just after the nozzle exit is necessary in order to design an efficient hydrogen injection system and injection strategies for optimised combustion. In the current study large-eddy simulations were performed to study the effect of different nozzle pressure ratios, namely 10, 30 and 70, on the near-nozzle shock structure and turbulent mixing of under-expanded hydrogen jets. The computational tool was validated against an experimental test case available in the literature. It was found that the simulation methodology captured the near-nozzle shock structure, Mach disk, reflected shocks and turbulent shear layers in good agreement with the experiments. The height and width of the Mach disk and the position of the mixing shear layer were greatly affected by the injection pressure. It was also found that for hydrogen the near-nozzle shock structure and Mach disk need considerably more time to reach an almost steady-state condition in comparison to the time claimed for heavier gases in the literature. It was also seen that during the transient period the dimensions of the Mach disk temporarily reached higher values than the final

steady ones. It was also found that not all of the hydrogen jet passed through the Mach disk; hydrogen-air mixing started immediately after the nozzle exit at the boundaries of the jet but the main mixing process started after the Mach disk.

NOMENCLATURE

| | | |
|--------------------|--------------------------------------|--|
| a | [-] | Face area vector |
| C_H | [-] | Empirical constant of the Mach disk height equation |
| C_p | [Jkg ⁻¹ K ⁻¹] | Specific heat |
| D | [mm] | Nozzle exit diameter |
| D_i | [m ² s ⁻¹] | Diffusion coefficient |
| F | [-] | Inviscid terms in <i>Navier-Stokes</i> equations |
| G | [-] | Viscous terms in <i>Navier-Stokes</i> equations |
| H | [-] | Body force |
| I | [-] | Identity matrix |
| P | [Pa] | Fluid pressure |
| P_0 | [bar] | Stagnation pressure |
| P_1 | [bar] | Nozzle exit pressure |
| P_∞ | [bar] | Ambient pressure |
| q | [Js ⁻¹] | Heat flux vector |
| R | [Jkg ⁻¹ K ⁻¹] | Gas constant |
| s | [Jkg ⁻¹ K ⁻¹] | Specific Entropy |
| S | [-] | Strain tensor |
| T | [-] | Transpose sign |
| T | [K] | Temperature |
| T_0 | [K] | Stagnation temperature |
| T | [-] | Viscous stress tensor |
| t_0 | [s] | Integral time scale |
| U | [ms ⁻¹] | Velocity magnitude |
| V | [ms ⁻¹] | Velocity vector |
| V_g | [ms ⁻¹] | Grid velocity vector |
| V | [m ³] | Computational cell volume |
| W | [-] | Conserved quantities in <i>Navier-Stokes</i> equations |
| Special characters | | |
| β | [°] | Reflected shock angle |
| γ | [-] | Ratio of specific heats |
| Δ | [m] | Length scale (LES grid filter) |
| ξ | [m] | Tip penetration ratio |
| ρ | [kgm ⁻³] | Density |
| μ | [m ² s ⁻¹] | Dynamic viscosity |
| μ_t | [m ² s ⁻¹] | Turbulent viscosity |
| σ_t | [-] | Turbulent Schmidt number |
| ∇ | [-] | Gradient operator |

INTRODUCTION

Due to the increasing price of the conventional fossil fuels (gasoline and diesel), supply uncertainty, and climate change issues, several liquids and gases have been suggested as cheaper and cleaner alternative fuels for internal combustion (IC) engines. Among them hydrogen (H_2) has been recommended as a promising alternative gaseous fuel for road transportation. The concept of a hydrogen economy and accordingly the idea of burning hydrogen in IC engines as a cleaner alternative to carbon-based fuels have been proposed since the mid-1970s [1, 2]. Experimental and computational studies have been conducted on developing hydrogen-fuelled IC engines predominantly since the beginning of the past decade [3–22]. Hydrogen is either injected in the port, *i.e.* port fuel injection (PFI) [6–12], or injected directly (DI) in the combustion chamber [13–22]. DI leads to higher volumetric efficiency and lower emissions in comparison to PFI and additionally avoids hydrogen abnormal combustion [13, 18]. Normally high pressures are used for DI of hydrogen in order to achieve high mass flow rate with fast mixing process particularly with injection strategies after intake valve closure. High injection pressures leads to choked conditions at the nozzle exit of the injector followed by a shock-containing under-expanded jet [18, 22]. Therefore, understanding the characteristics of under-expanded hydrogen jets and the near-nozzle shock structure are necessary in order to study the mixture formation in DI hydrogen-fuelled IC engines.

Characteristics of a gaseous jet issuing from a circular nozzle are highly dependent on the ratio of the nozzle total pressure (P_0) to the ambient static pressure (P_∞), namely the nozzle pressure ratio (NPR). Based on NPR , jets can be categorized as subsonic, moderately under-expanded and highly under-expanded. For NPR above ~ 4 the issuing jet is considered to be highly under-expanded. As illustrated in Figure 1, at such condition, an expansion fan forms at the nozzle lip that spreads out to the jet boundary and reflects as weak compression waves which form the intercepting oblique shock ended by a slightly curved strong normal shock so-called Mach disk [23]. The oblique shock and the Mach disk form the first shock cell that is termed “barrel shape shock” since it has a cylindrical form. The oblique shock and the Mach disk merge at the triple point and produce a reflected shock and a slip line. The flow behind the Mach disk is subsonic, whilst the flow behind the reflected shock is still supersonic [23, 24]. For higher degrees of under-expansion, *e.g.* $NPR \sim 8$, the subsonic core behind the Mach disk is rapidly accelerated and becomes supersonic again which then shapes a second shock cell that may resemble the first shock cell and even include a normal shock similar to the Mach disk [25]. At very high NPR a Mach disk with large height forms at the nozzle exit with no other normal shocks downstream and the jet decays through a structure of oblique shocks [25].

Location of the Mach disk and dimensions of the intercepting shock in under-expanded jets have been investigated both experimentally and computationally since the mid-1950s mainly for aerospace and aeronautical

applications. Experimental studies have been conducted by several researches using Schlieren and shadowgraph photography, Rayleigh scattering, Laser Doppler Anemometry (LDA) and Planar laser-induced fluorescence (PLIF) in order to visualise the near-nozzle shock structure and mixing parameters of under-expanded air/nitrogen jets [26–33]. Computational studies by means of *Reynolds* Averaged *Navier-Stokes* (RANS) and large eddy simulation (LES) have also been conducted mainly on under-expanded air jets or by assuming the injection of a passive scalar [34–39].

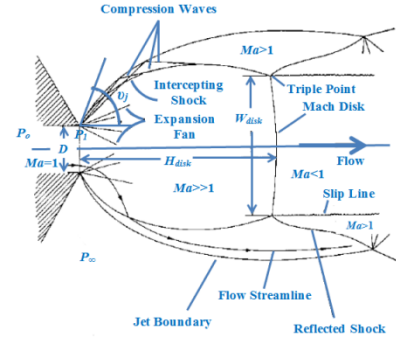


Figure 1 Schematic of near-nozzle structure of under-expanded jets. The picture is based on the visualisation presented by Crist *et al* [23]

Crist *et al* [23] used a hot-shot wind-tunnel facility and Schlieren to study the near nozzle shock structure and to measure the position of the Mach disk for a variety of gases including Nitrogen, Argon, Helium, and CO_2 under NPR s up to 100,000. Various nozzle exit diameters (0.66–3.0 mm) were investigated. They found that the location of the Mach disk was weakly sensitive to the ratio of specific heats γ and insensitive to solid boundary geometry at the nozzle lip and absolute pressure level, while NPR was the only parameter to determine the Mach disk location. Crist *et al* [23] then concluded that the relation between NPR and Mach disk height can be described as,

$$\frac{H_{disk}}{D} = C_H \sqrt{P_0/P_\infty} \quad (1)$$

The constant C_H in equation (1) was derived to be ~ 0.645 . Crist *et al* [23] also observed that the Mach disk diameter, jet boundary and intercepting shock increase with decrease in the ratio of specific heats, and decrease at very high upstream stagnation densities (~ 200 times atmospheric for N_2) where intermolecular forces become dominant [23].

There are very limited studies available in the literature on under-expanded hydrogen jets. Ruggles and Ekoto [40] used Schlieren photography to visualise near nozzle shock structure and also used Planar Laser Rayleigh Scatter imaging to measure instantaneous mole fractions downstream of the Mach disk in an under-expanded hydrogen jet with NPR of 10 issued from a nozzle with a diameter of $D=1.5$ mm. The Mach disk and the reflected shocks, in addition to the oblique shock

trains after the Mach disk, were clearly captured by the visualisation technique. Ruggles and Ekoto [40] noticed that air and issuing hydrogen may have mixed within the slip region but suggested that more experimental and computational works were required in order to clarify the hydrogen mixing behaviour very close to the nozzle exit. Gorle *et al* [41] and Gorle and Iaccarino [42] conducted experimental (Schlieren) and computational (RANS and LES) studies of under-expanded hydrogen jets issuing from a nozzle with $D=2$ mm and NPR of 30. They noticed that both RANS and LES were able to capture the near nozzle shock structure in good agreement with experiments. Khaksarfard *et al* [43] numerically investigated the release of very high pressure hydrogen (10–70 MPa) into atmospheric ambient through a circular release hole with $D=5$ mm. They used a *Noble-Abel* real gas equation of state (EoS) and found that for very high injection pressures the ideal gas equation underestimates the release velocity and that for injection pressure above 10 MPa a real gas equation must be used to obtain accurate results. Recently Bonelli *et al* [45] used a modified $k-\epsilon$ RANS model with 3 different EoS, namely ideal gas, *van der Waals*, and *Redlich-Kwong* in order to study high pressure injection of hydrogen (75 MPa) issuing into still nitrogen (5 MPa) through a nozzle with inner and outer diameter of 0.3 mm and 0.6 mm respectively. Similarly to Khaksarfard *et al* [44] they noticed that the ideal gas EoS over-predicted the mass of the injected hydrogen by 10% and 8.7% in comparison to the *van der Waals* and *Redlich-Kwong* formulations respectively. Additionally, Bonelli *et al* [45] noticed that at very high injection pressures ($P_0 > 100$ bar) the ideal gas EoS overestimated the mass flow rate; in contrast a smaller Mach disk height was noticed when a real gas EoS was applied.

Although a considerable amount of work has been devoted to improve the understanding of under-expanded jets there has been a lack of research focusing on under-expanded hydrogen jets particularly for IC engine applications. In the present work computational simulations were performed on under-expanded hydrogen jets with different values of NPR , namely 10, 30 and 70, using LES. The computational tool was validated against an experimental test case available in the literature [40]. The near-nozzle shock structure and turbulent mixing of under-expanded hydrogen jets were investigated.

COMPUTATIONAL METHODOLOGY

The viscous flow of a Newtonian multi-component fluid of N species ($Y_1, Y_2, Y_3, \dots, Y_i, \dots, Y_N$) is governed by the *Navier-Stokes* equations and species transport equation that in a *Cartesian* integral form can be written as equations (2) and (3) respectively [45, 46]:

$$\frac{\partial}{\partial t} \int_V \mathbf{W} dV + \oint [\mathbf{F} - \mathbf{G}] \cdot d\mathbf{a} = \int_V \mathbf{H} dV \quad (2)$$

where:

$$\begin{aligned} \mathbf{W} &= \begin{bmatrix} \rho \\ \rho \mathbf{V} \\ \rho E \end{bmatrix}, & \mathbf{F} &= \begin{bmatrix} \rho(\mathbf{V} - \mathbf{V}_g) \\ \rho(\mathbf{V} - \mathbf{V}_g) \otimes \mathbf{V} + P\mathbf{I} \\ \rho(\mathbf{V} - \mathbf{V}_g)H + P\mathbf{V}_g \end{bmatrix} \\ \mathbf{G} &= \begin{bmatrix} 0 \\ \mathbf{T} \\ \mathbf{T} \cdot \mathbf{V} + \dot{q} \end{bmatrix}, & \mathbf{H} &= \begin{bmatrix} S_u \\ \mathbf{f}_r + \mathbf{f}_g + \mathbf{f}_p + \mathbf{f}_u + \mathbf{f}_\omega \\ S_u \end{bmatrix} \\ & & & \frac{\partial}{\partial t} \int_V \rho Y_i dV + \oint_A \rho Y_i (\mathbf{V} - \mathbf{V}_g) \cdot d\mathbf{a} = \\ & & & \int_A \left[\left(D_i + \frac{\mu_t}{\sigma_c} \right) \nabla Y_i \right] \cdot d\mathbf{a} \end{aligned} \quad (3)$$

For N species, $N-1$ transport equations are solved and the mass fraction of the N^{th} component is calculated from the restriction that the total mass fraction must sum to unity. Pressure is coupled to the density and temperature via the ideal gas EoS. For the current study the STAR-CCM+ code was used. The code applies a coupled finite volume (FV) model that discretises and solves the governing equations simultaneously using an implicit time marching approach. To provide efficient solution a preconditioning matrix is integrated into equation (2) that consequently requires viscous and inviscid fluxes to be defined. The viscous fluxes can be written in terms of the stress tensor \mathbf{T} which is defined as equations (4), (5) using *Boussinesq's* approximation [45]. In order to express the inviscid fluxes a modified version of advection upstream splitting method (AUSM⁺) is applied which is believed to be accurate and robust in solving fluid flows that contain discontinuity such as shock waves [47, 48]:

$$\mathbf{T} = \mathbf{T}_{laminar} + \mathbf{T}_{turbulent} \quad (4)$$

$$\mathbf{T} = (\mu + \mu_t) \left[\nabla \mathbf{V} + \nabla \mathbf{V}^T - \frac{2}{3} (\nabla \cdot \mathbf{V}) \mathbf{I} \right] \quad (5)$$

Since solving the governing equations directly (*i.e.* using direct numerical simulation (DNS) for the complicated flow that is investigated in this work is not feasible at the time due to the lack in computational power, LES which requires coarser grid is used. In LES the governing equations are filtered in a way that the turbulence scales greater than the grid resolution are solved directly and the smaller scales are modelled using special approximations namely sub-grid scale (SGS) models. SGS model is required in order to define the turbulent viscosity (μ_t) that is used in equation (6) to calculate the turbulent stress tensor ($\mathbf{T}_{Turbulent}$):

$$\mathbf{T}_{Turbulent} = 2\mu_t \mathbf{S}_3^2 (\mu_t \nabla \cdot \mathbf{V} + \rho k) \mathbf{I} \quad (6)$$

where \mathbf{S} is the strain rate tensor computed from the resolved velocity field as:

$$\mathbf{S} = \frac{1}{2} (\nabla \mathbf{V} + \nabla \mathbf{V}^T) \quad (7)$$

In the current work wall-adapting local-eddy viscosity (WALE) [49] sub-grid scale was applied. In this model μ_t is approximated using equation (8):

$$\mu_t = \rho \Delta^2 S_w \quad (8)$$

where Δ is the length scale or grid filter width and S_w is the deformation parameter and is a function of the strain rate tensor. The current computational framework was second-order accurate for both temporal and spatial discretizations.

Simulations of highly under-expanded hydrogen jets were performed by considering a system that consisted of a high pressure hydrogen tank and a low pressure air-containing chamber that were linked using a converging nozzle with exit diameter $D=1.5$ mm, as can be seen in Figure 2. Overall three simulations were carried out for three different NPRs; 10, 30, and 70. The pressure of the low pressure chamber was kept constant for the three simulations at 98.37 kPa, whereas the temperature of both the high pressure hydrogen tank and the low pressure chamber were kept constant at 295.4 K and 296 K, respectively. The top boundary of the high pressure hydrogen tank was considered a stagnation inlet, while the side and the bottom boundaries of the low pressure chamber were set to pressure outlet. Following practices in the literature [35, 37], the rest of the boundaries, including the wall of the converging nozzle, were set to adiabatic slip in order to avoid formation of any artificial boundary layers. Additionally, the turbulent boundary layer at such high speeds would be very thin and this would require a very fine grid close to the wall to resolve the turbulent structure down to the viscous sublayer.

For the current study an unstructured hexahedral grid was created using the trimmer facility of STAR-CCM+ that produces cubic cells with identical size in all dimensions. As it can be seen in Figure (2) in order to capture the flow details inside the nozzle, the shock structure very close to the nozzle exit and the mixing process downstream of the nozzle, a conical refined area was implemented inside the computational grid that covered the nozzle volume and a length of $20D$ downstream of the nozzle exit. This refined area very close to the nozzle exit (within a distance of $\sim 6.7D$) and inside the nozzle volume had a cell size of ~ 0.03 mm ($D/50$) while further downstream it had a cell size of ~ 0.06 mm. the cell size from the refined area expands toward the largest cell size inside the domain (1.0 mm) through a near four level of grid expansion.

The simulations started from the rest condition where it was assumed that hydrogen occupied the entire high pressure tank and vary small part of the converging nozzle volume up to $\sim 1.4D$ above the nozzle exit. Air occupied the low pressure chamber and remaining of the nozzle volume. The length of the high pressure hydrogen tank is believed to be long enough ($40D$) so that the flow can be considered to be almost at rest at the stagnation inlet. This assumption eliminates the need for applying any initial perturbation at the inlet boundary for LES studies. Since just two species, *i.e.* hydrogen and air, were involved in the current study, the molecular diffusivity D_i in equation (3) was defined as binary diffusivity of air-hydrogen system which was calculated using *Chapman-Enskog* theory for gaseous diffusion coefficients [50] and was calculated to

be $D_i = 7.942 \times 10^{-5}$ m²/s. The nominal integral time scale of an under-expanded gaseous jet issued from a circular nozzle can be defined as $t_0 = D/2U_{exit}$, *e.g.* according to the work of [37]. This definition was also employed in the current work for comparison purposes. Assuming choked condition ($Ma=1$) at the nozzle exit of the present work, t_0 was about 6.2×10^{-17} s. All simulations were conducted for a duration of about $162t_0$ each, *i.e.* ~ 0.1 ms. A time-step of 5.0×10^{-9} s was used at the beginning of the simulations, which was then increased to 5.0×10^{-8} s for the rest of the simulation time. This value was almost 10 times smaller than the nominal integral time scale of the flow and it was considered adequate for capturing the turbulent temporal fluctuations in satisfactory detail within feasible CPU times.

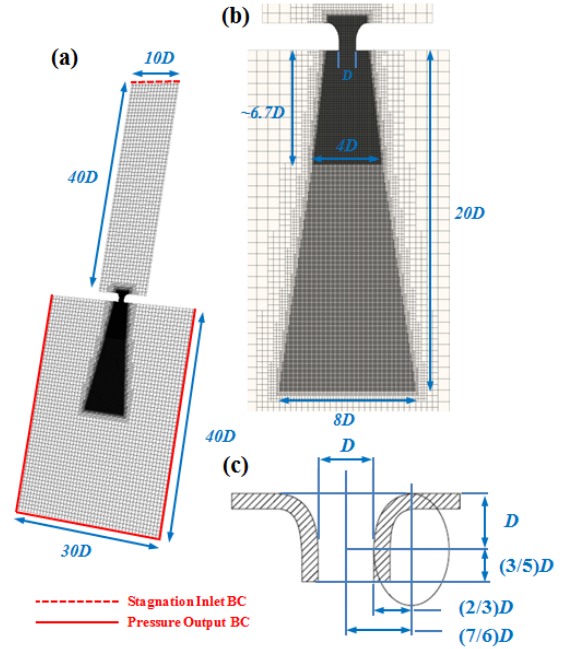


Figure 2 (a) Section view of the grid and the domain dimensions. (b) Zoomed view of the refined areas. (c) Nozzle profile and its dimensions based on Ruggles and Ekoto [40]

Model Validation

In order to validate the computational framework a test case with $NPR=10$ was setup based on the experimental work of Ruggles and Ekoto [40]. The nozzle geometry shown in Figure 2 was specifically designed according to data in [40]. Figure 3 compares the LES results of the current study with the Schlieren images presented by Ruggles and Ekoto [40]. The LES image is based on the magnitude of the density gradient $|\nabla\rho|$ and a grey scale legend was used in order to provide better visualisation of the shock structures.

As shown in Figure 3, the Mach disk height and width, as well as the reflected shock angle, were predicted by LES very close to values that can be extracted from the Schlieren image. According to Ruggles and Ekoto [40] the Mach disk height and width were 3.05 mm and 1.30 mm, respectively, whereas the current LES study predicted values higher by just 1.3% and 3.0% for these two parameters (3.09 mm and 1.34 mm,

respectively). Similarly to the experiments [40], the current LES study predicted the reflected shock (at the triple point) to be inclined 28° against the nozzle centreline axis; slip lines were also similarly predicted. As it was pointed out by Ruggles and Ekoto [40], LES also showed that hydrogen and air are mixing outside of the shock structures and that not all of the hydrogen passed through the Mach disk.

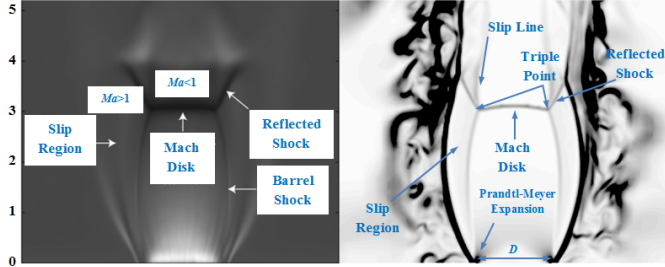


Figure 3 Near nozzle shock structure. Left: Schlieren [40]. Right: Current LES study

It has been shown in [37] that the tip penetration of under-expanded jets Z_{tip} can be related to the nominal time scale t_0 as follows:

$$\xi = \frac{Z_{tip}}{(\rho_0/\rho_\infty)^{0.25}} \sim \left(\frac{t}{t_0}\right)^{0.5} \quad (9)$$

If ξ is plotted against $(t/t_0)^{0.5}$, the data is expected to collapse almost into a linear relationship [37]. Figure 4 shows this relationship for two hydrogen jets of the current study with $NPR=8.5$ and 10 , as well as for the nitrogen passive scalar work of [37]. It is clear that all three collapse for $t/t_0 > 49$. The differences for $t/t_0 < 49$ are related to the specific behaviour of the two types of gases during the initial transient development of the jet.

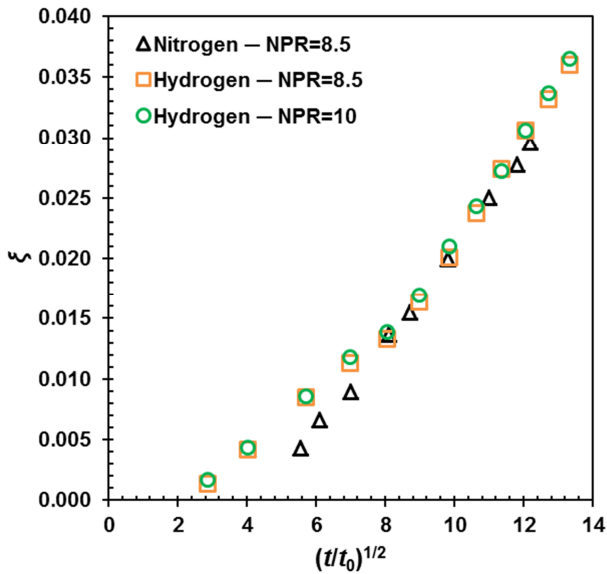


Figure 4 Normalized jet tip penetration. Comparison between hydrogen jets of the current LES study with a nitrogen jet available in the literature [37].

RESULTS AND DISCUSSION

Early stages of near-nozzle shock development and Mach disk formation for the $NPR=10$ case is presented in Figure 5. At $t=13t_0$ the *Prandtl-Meyer* expansion fans resulted in formation of a spherically propagating bow shock, followed by the growth of the first oblique shocks. Soon after that at $t=21t_0$, when the nozzle exit pressure P_1 reached the threshold of under-expansion, *i.e.* $P_1/P_\infty > 2$, a very small normal shock with narrowly spaced slip lines formed close to the nozzle exit. This small normal shock can be assumed as the first appearance of the Mach disk. As time passed, the distance between slip lines grew and the width of the Mach disk increased. At $t=32t_0$ the width of the Mach disk was slightly wider than the nozzle exit diameter D and the barrel shape of the first shock cell could be identified. After this point the size of the Mach disk height and width started fluctuating around their final steady values. At $t=113t_0$ the near nozzle shock structure and height and width of the Mach disk reached a steady condition and no further fluctuation was observed. At this steady condition the values of the Mach disk's height and width were 3.09 mm and 1.34 mm, respectively, as also pointed out earlier in the validation section. As it is clear in Figure 5, the current LES framework was able to capture the emitted sound waves from the under-expanded hydrogen jet. Turbulence instabilities and hydrogen/air mixing was observed outside of the barrel shape shock cell that was related to the high turbulence level at the nozzle exit. From Figure 5 it can be concluded that the main hydrogen/air mixing process starts after the Mach disk and the intensity of the turbulence increase further downstream particularly at the jet boundary.

Instantaneous spatial variations of H_2 mole fraction, Mach number, temperature and velocity for $NPR=10$ at $t \approx 161t_0$ are presented in Figure 6. As it can be seen from the mole fraction snapshot, the maximum tip penetration of the jet can occur at a location within a radial distance away from the nozzle centreline axis. Air/hydrogen mixing outside the first shock cell is as shown earlier in Figure 5. Due to the rapid expansion of the jet, the Mach number reaches a maximum value of $Ma \approx 3.98$ in the vicinity of the Mach disk. As it will be described later, the Mach number at the nozzle exit in steady condition was $Ma \approx 1.1$. Formation of at least 3 small shock cells after the Mach disk is visible in the Mach snapshot of Figure 6.

As it can be seen in the temperature snapshot of Figure 6, using ideal gas EoS predicts a temperature of ~ 70 K just before the Mach disk and a temperature very close but lower than the ambient temperature (~ 296 K) just after the Mach disk location. It is believed that due to the negative *Joule-Thomson* coefficient of hydrogen the temperature profile very close to the nozzle exit cannot be predicted accurately using an ideal gas EoS. As it has been presented by some researchers [43, 44], using a real gas EoS like *Redlich-Kwong*, results in capturing a higher temperature than the ambient one just after the Mach disk. The effect of using a real gas EoS on under-expanded hydrogen jets is under on-going study by the

current authors and it will be discussed in a future publication. Figure 6 also shows that the jet velocity at the nozzle exit was calculated to be about $U_{\text{exit}} \approx 1310$ m/s and the jet velocity reached to a maximum value of about $U \approx 2540$ m/s just before the Mach disk.

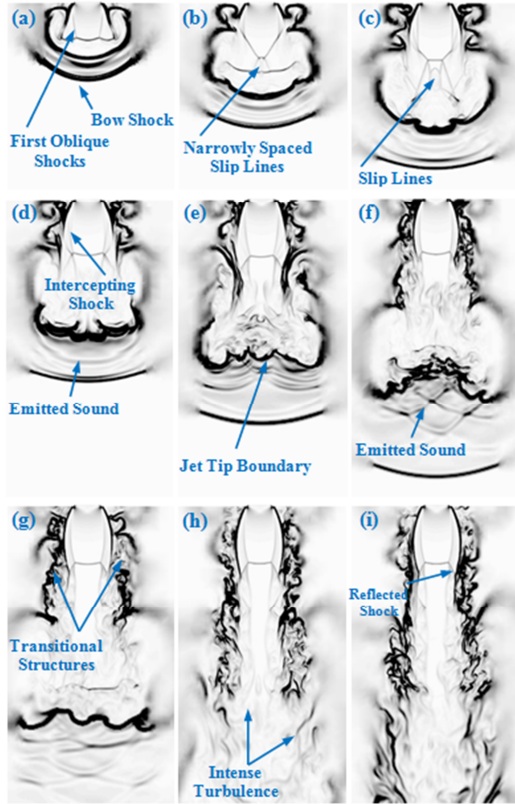


Figure 5 LES prediction of near nozzle shock structure, Mach disk formation and turbulent mixing in under-expanded hydrogen jet with $NPR=10$. These images are based on the magnitude of density gradient $|\nabla\rho|$. (a): $\sim 13t_0$, (b): $\sim 21t_0$, (c): $\sim 29t_0$, (d): $\sim 32t_0$, (e): $\sim 40t_0$, (f): $\sim 51.5t_0$, (g): $\sim 63t_0$, (h): $\sim 113t_0$, (i): $\sim 161t_0$

In addition to the test case with $NPR=10$, two more cases with NPR of 30 and 70 were investigated. Figure 7 shows a comparison between results for $NPR=10$ and $NPR=30$. It is clear that the Mach disk dimensions are noticeably larger for $NPR=30$ in comparison to the case with $NPR=10$. The Mach disk height and width for $NPR=30$ are 5.43 mm and 2.95 mm, respectively, which corresponds to an increase of $\sim 75\%$ and $\sim 120\%$, respectively, in comparison to the test case with $NPR=10$. It should be noted that for hydrogen jets with NPR values of 30 and 70 the Mach disk did not reach a final steady state size within the simulated time of $t \approx 161t_0$. As mentioned earlier for the jet with $NPR=10$, the Mach disk height and width for $NPR=30$ and 70 could reach values larger than the expected steady ones, but it is believed that the final steady values should be close to those presented in Table 1, as obtained at $t \approx 161t_0$ and as can be obtained from empirical relations such as equation (1). As illustrated in Figure 7, the values of the angle β of the reflected shock at the triple point

for the test cases with NPR of 10 and 30 are the same and equal to $\beta \approx 28^\circ$. Further characteristics of the under-expanded hydrogen jets investigated in the current study are tabulated in Table 1. The near-nozzle shock structure for $NPR=70$ was not visualised since the Mach disk width in this case was bigger than the width of the refined area of the computational grid and it was not possible to have a clear quantification of the reflected shock structure and the slip lines. However, it is believed that the angle of the reflected shocks remains constant at $\beta \approx 28^\circ$ even beyond $NPR=30$, *i.e.* it becomes independent of NPR as also commented in the literature at different conditions to those of the current study [37]. It was noticed that increasing NPR from 30 to 70 increased the Mach disk height by $\sim 51\%$. Data from Table 1 were used to calculate the constant C_H by reordering equation (1); values of 0.651 and 0.66 were calculated for $NPR=10$ and $NPR=30$, respectively. These are very close to the values of 0.645 claimed by Crist *et al* [23]. It is also worth mentioning that calculating the constant C_H for $NPR=70$ with the same procedure gave a value of $C_H \approx 0.655$ that highlighted a need for further investigation, probably by applying a real gas EoS. It has already been claimed that the use of real EoS is necessary for $P_0 > 100$ bar [44].

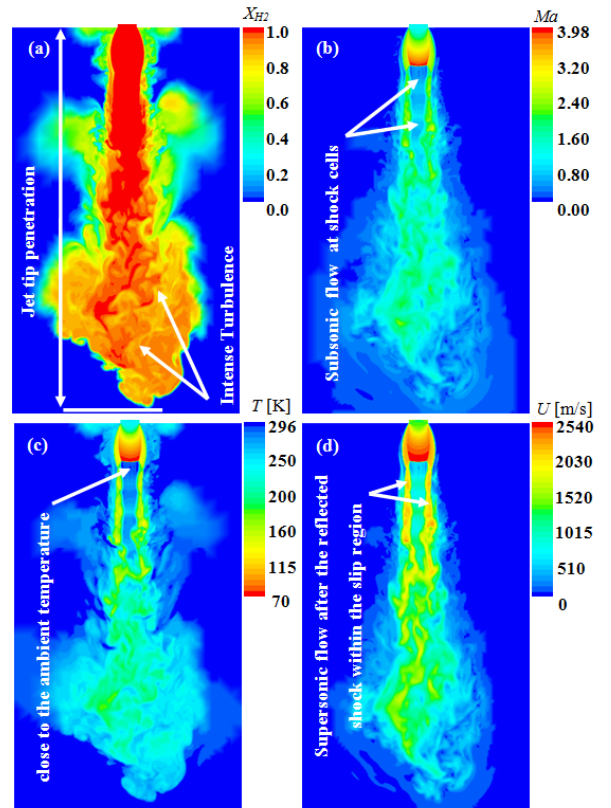


Figure 6 Instantaneous snapshots of various flow quantities for the $NPR = 10$ at $t \approx 161t_0$. (a): Mole fraction of H_2 , (b): Mach number, (c): Temperature, (d): Velocity

It was observed that shortly after the start of injection (for instance $t=30-40t_0$ for $NPR=10$) the maximum tip penetration of H_2 occurred at positions within a noticeable distance from

the nozzle centreline (see Figure 5). This is believed to be the transient effect of the formation of Mach disk and centreline shock cells. The distance reduced as the jet penetrated more and, for example, for $NPR=10$ at $t \approx 70t_0$ this distance reached a value less than the nozzle diameter D . After this time the distance between maximum jet tip penetration and centreline penetration started ranging between values less than $\sim 0.75D$. It was also observed that for higher NPR longer time was required for both penetrations to occur within the mentioned threshold and it is clear from Table (1) that even at $t \approx 161t_0$ this did not happen for $NPR=70$.

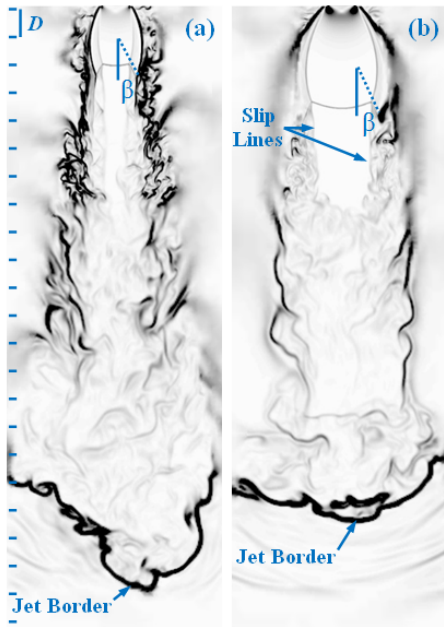


Figure 7 Shock structure and turbulence characteristics of under-expanded H_2 jets for (a): $NPR=10$, (b): $NPR=30$.

If it is assumed that the jet with $NPR=70$ followed the same trend as the other two jets did, then at later time steps the jet centreline penetration for $NPR=70$ would be higher than that of $NPR=30$. Higher jet penetration provides faster fuel/air mixing in hydrogen-fuelled IC engines and, based on Table 1, it is clear that increasing the NPR does not necessarily increase the jet penetration since the jet with $NPR=10$ penetrated $\sim 13\%$ more than the jet with $NPR=30$. A similar trend was noticed by Owston *et al* [51] where jets with identical mass flow rate, $NPR \approx 20$ produced lower penetration than $NPR \approx 10$. They concluded that insufficient grid resolution caused this to occur [51]. However, in the current study where according to the literature [35, 37] the grid resolution was fine enough to capture the details of under-expanded jets, a similar trend was observed even for jets with different mass flow rates. Therefore, it can be postulated that there would be a trade-off between the width and penetration of the jets and there should be an optimum NPR that can provide a desirable penetration. According to Table 1 $NPR=100$ may be suggested as the optimum value since it would produce a higher penetration compared to $NPR=10$, whilst delivering more fuel in less time. The initial transient penetration phase was studied

in the current work because it is very important for hydrogen DI engine applications. Depending on the injector position and injection strategy, the distance travelled by the jet before impinging onto the cylinder liner or the piston crown can range typically from ~ 20 – 80 mm [18, 22] which is within the values shown in Table 1. However, more work is required with longer injection times both for IC engine conditions and hydrogen safety related applications.

Table 1 Characteristics of H_2 jets at $t=161t_0$

| NPR | Mach Disk Height | Mach Disk Width | Second Shock Cell Length | Tip Penetration | Centreline Penetration |
|-------|------------------|-----------------|--------------------------|-----------------|------------------------|
| [-] | [mm] | [mm] | [mm] | [mm] | [mm] |
| 10 | 3.09 | 1.34 | 4.035 | 30.78 | 29.70 |
| 30 | 5.43 | 2.95 | 5.775 | 27.11 | 26.72 |
| 70 | 8.23 | NA | No Cell | 28.65 | 23.97 |

The centreline Mach number and density at $t \approx 161t_0$ are plotted against the normalised distance from the nozzle exit (Z/D) in Figures 8 and 9, respectively. It is clear from Figure 8 that for all NPR s the Mach number at the nozzle exit is ~ 1.1 . Studying the transient jets from the start of injection revealed that at the early stages of injection a subsonic jet started issued from the nozzle exit, then the flow accelerated and reached $Ma=1$ at the nozzle exit. When the Mach disk started forming, the flow inside the nozzle reached a value of $Ma=1$ upstream the nozzle exit. The position of $Ma=1$ moves backwards upstream, associated by an increase in the size of the Mach disk. When the Mach disk and shock structure close to the nozzle exit reached semi steady conditions, $Ma=1$ occurred $\sim 0.5D$ upstream the nozzle exit; a maximum Mach number of $Ma \approx 1.3$ occurred $\sim 0.2D$ upstream of the nozzle exit. From the time that the location of $Ma=1$ started occurring inside the nozzle, it was noticed that the Mach number dropped again with a slope that increased in time in such a way that the nozzle exit Mach number ranged from ~ 1.01 at the beginning of the Mach disk formation to ~ 1.1 when the Mach disk dimensions had reached a semi-steady condition. A Mach number higher than unity at the nozzle exit, $Ma \approx 1.2$, was also observed in the work of Khaksarfard *et al* [43] where hydrogen was injected with pressure of $P_0=34.5$ MPa into atmospheric ambience. However, in [43], the authors presented results for an injection duration of $25 \mu s$ which was not long enough to capture the peak of the Mach number and the transient in-nozzle flow in the same way that this behaviour was captured by the current study (see Figure 8). By performing computational studies of high pressure injection of nitrogen in an ejector (vacuum jet), Zhu and Jiang [52] captured a behaviour of the in-nozzle Mach number that was very close to the current study.

In Figure 8 the Mach number behaviour just before the nozzle exit may look like a normal shock phenomenon but, as

illustrated in Figure 10, the aforementioned transient process did not produce much entropy increase since it took place gradually during time, unlike the formation of the Mach shock which produced a sudden drop in the Mach number and other flow parameters from its first appearance. The specific entropy in Figure 10 was calculated using equation (10) where the reference parameters P_0 and T_0 were set to their stagnation values of hydrogen inside the fuel reservoir. The stagnation temperature was assumed to be $T_0=295.4$ K for all test cases whereas the value of the stagnation pressure P_0 was ~ 9.8 , ~ 29.5 , and ~ 69.0 bar for NPR values of 10, 30 and 70 respectively.

$$s = C_p \ln\left(\frac{T}{T_0}\right) - R \ln\left(\frac{P}{P_0}\right) \quad (10)$$

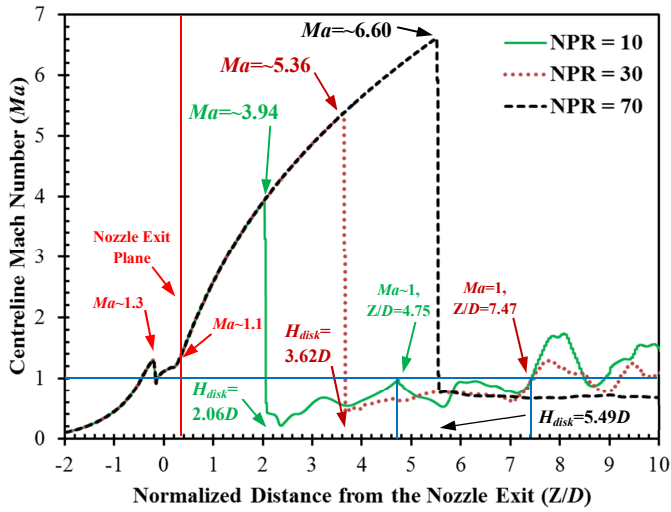


Figure 8 Variation of Mach number along the nozzle centreline axis at $t \approx 161t_0$

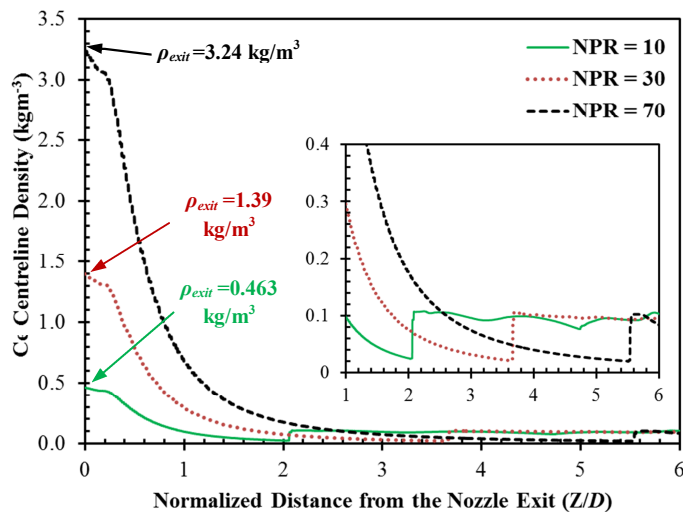


Figure 9 Variation of Density (ρ) along the nozzle centreline axis at $t \approx 161t_0$

The maximum value of the Mach number that happened at the vicinity of the Mach disk was 3.94, 5.36, and 6.60 for NPR of 10, 30, and 70 respectively. From Figure 8 it is clear that the length of the subsonic core just after the Mach disk increased by increasing the NPR . For NPR values of 10 and 30 the flow reached $Ma=1$ at normalised distance from the nozzle exit (Z/D) of 4.75 and 7.47, respectively. For $NPR=70$, as also mentioned earlier, due to the very strong normal shock the flow could not reach $Ma=1$ past the Mach disk and remained subsonic. The nozzle exit velocity for all values of NPR was about $U \approx 1310$ m/s. The values of density at the nozzle exit (Figure 9) led to mass flow rates of 1.07, 3.21 and 7.50 g/s for NPR values of 10, 30 and 70, respectively. The calculated mass flow rate for $NPR=10$ is in a good agreement with the value of ~ 1.0 g/s reported by Ruggles and Ekoto [40] from their experimental data obtained at the same conditions to those of the current study.

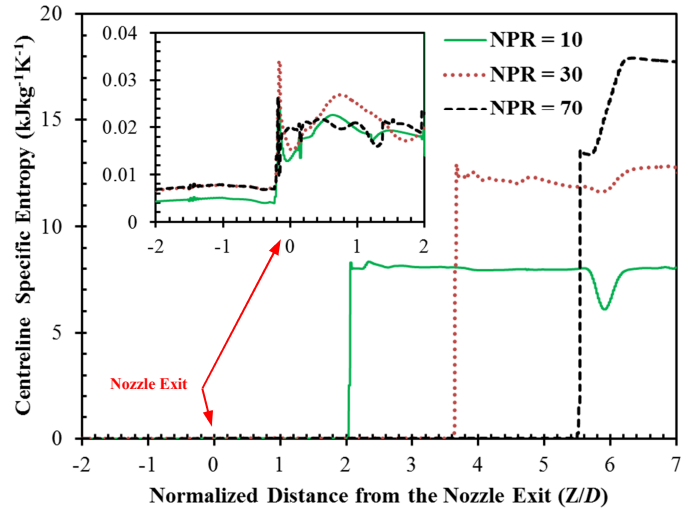


Figure 10 Variation of specific entropy (s) along the nozzle centreline axis $t \approx 161t_0$

CONCLUSIONS

The current study focused on LES of under-expanded hydrogen jets under different values of NPR , namely 10, 30, and 70, for injection duration of $100\mu s$. The computational framework was validated against an experimental test case available in the literature. The near nozzle shock structure and mixing characteristics of hydrogen jets were then investigated. The Mach disk height and width, as well as the angle of the reflected shock at the triple point and the length of the subsonic core after the Mach disk were studied quantitatively. The main conclusions can be summarized as follows:

- The height and width of the Mach disk were very sensitive to NPR . A higher degree of sensitivity to NPR was noticed for the width of the disk than for the height. The height of the Mach disk was $\sim 2.06D$, $\sim 3.62D$ and $\sim 5.49D$ for NPR equal to 10, 30 and 70, respectively. The width of the Mach disk for $NPR=10$ and 30 was $\sim 0.89D$ and $\sim 1.97D$, respectively.

- By increasing the *NPR* from 10 to 70, the angle of the reflected shock at the triple point remained constant at about 28°.
- By increasing the *NPR* from 10 to 30, the length of the subsonic core just after the Mach disk increased from ~4 mm to ~5.8 mm, *i.e.* by ~45%. At *NPR*=70 the subsonic core did not turn sonic and continued decaying in a subsonic manner after the Mach disk.
- Applying higher *NPR* did not necessarily increase the penetration of the jet. Therefore, there should be an optimum *NPR* that can provide the desirable penetration under a certain design brief; a value of 100 may be the optimum *NPR* for the conditions of the present study. However, further work is required for a solid conclusion.
- Studying the transient jets with different values of *NPR* revealed that at the beginning of injection a subsonic jet formed at the nozzle exit. Then the flow accelerated inside the nozzle and at the nozzle exit it reached $Ma=1$. When the Mach disk started forming, the location of $Ma=1$ moved upstream of the nozzle exit and at semi-steady conditions the Mach number at the nozzle exit for all values of *NPR* was ~1.1.
- At the semi-steady condition it was observed that the maximum Mach number inside the nozzle was ~1.3. This occurred at ~0.2*D* upstream of the nozzle exit. After this point *Ma* decreased to ~0.8 at ~0.15*D* upstream of the nozzle exit and again increased to ~1.1 at the nozzle exit.
- The jet's development from subsonic condition to under-expanded steady condition did not produce noticeable entropy change inside the nozzle since the procedure occurred gradually. However, the formation of the Mach disk, even from its early stages, produced a large increase in entropy in the vicinity of the shock since the thermodynamic conditions changed suddenly at the Mach disk location.
- It was noticed that not all the hydrogen passed through the Mach disk and that part of the jet bypassed the disk. For *NPR*=10, hydrogen/air mixing started at the boundaries of the slip region before the Mach disk. This was due to high levels of turbulence at the nozzle exit. A wider grid refinement area was required to study this specific mixing region for *NPR* values of 30 and 70.
- For all values of *NPR* the main hydrogen/air mixing was observed to start after the Mach disk location and particularly closer to the jet boundary where intense turbulence was noticed to play a dominant role in the mixing process.

ACKNOWLEDGMENTS

The authors acknowledge the use of University College London's Legion High Performance Computing Facility (Legion@UCL), and associated support services, in the completion of this work. The authors would also like to thank all members of the UCL Internal Combustion Engines Group for their assistance and many useful discussions.

REFERENCES

- [1] Bokris J. O'M., The Origin of Ideas on a Hydrogen Economy and its Solution to the Decay of the Environment, *International Journal of Hydrogen Energy*, Vol.27, 2002, pp. 731–740.
- [2] Lattin W.C., and Utgikar V.P., Transition to hydrogen economy in the United States: A 2006 status report, *International Journal of Hydrogen Energy*, Vol.32, 2007, pp. 3230–3237.
- [3] White C.M., Steeper R.R., and Lutz A.E., The hydrogen-fueled internal combustion engine: A technical review, *International Journal of Hydrogen Energy*, Vol.31, 2006, pp. 1292–1305.
- [4] Verhelst S., and Wallner T., Hydrogen-fueled internal combustion engines, *Progress in Energy and Combustion Science*, Vol.35, 2009, pp. 490–527.
- [5] Al-Baghdadi M., and Al-Janabi H.A., A prediction study of a spark ignition supercharged hydrogen engine, *Energy Conversion and Management*, Vol.44, 2003, pp. 3143–3150.
- [6] Berckmüller M., Rottengruber H., Eder A., Brehm N. et al., Potentials of a Charged SI-Hydrogen Engine, *SAE Technical Paper* 2003-01-3210, 2003.
- [7] Verhelst S., and Sierens R., Combustion Studies for PFI Hydrogen IC Engines, *SAE Technical Paper* 2007-01-3610, 2007.
- [8] Verhelst S., Maesschalck P., Rombaut N., and Sierens R., Increasing the power output of hydrogen internal combustion engines by means of supercharging and exhaust gas recirculation, *International Journal of Hydrogen Energy*, Vol.34, 2009, pp. 4406–4412.
- [9] Kawahara N., and Tomita E., Visualization of auto-ignition and pressure wave during knocking in a hydrogen spark-ignition engine, *International Journal of Hydrogen Energy*, Vol.34, 2009, pp. 3156–3163.
- [10] Rakopoulos C.D., Kosmadakis G.M., and Pariotis E.G., Evaluation of a combustion model for the simulation of hydrogen spark-ignition engines using a CFD code, *International Journal of Hydrogen Energy*, Vol.35, 2010, pp. 12545–12560.
- [11] Rakopoulos C.D., Kosmadakis G.M., Demuyneck J., De Paepe M., and Verhelst S., A combined experimental and numerical study of thermal processes, performance and nitric oxide emissions in a hydrogen-fueled spark-ignition engine, *International Journal of Hydrogen Energy*, Vol.36, 2011, pp. 5163–5180.
- [12] Aleiferis P.G., and Rosati M.F., Flame chemiluminescence and OH LIF imaging in a hydrogen-fuelled spark-ignition engine, *International Journal of Hydrogen Energy*, Vol.37, 2012, pp. 1797–1812.
- [13] Kaiser S. and White C., PIV and PLIF to Evaluate Mixture Formation in a Direct-Injection Hydrogen-Fuelled Engine, *SAE Int. J. Engines*, 2009, pp. 657–668.
- [14] Wallner T., Nande A., and Naber J., Evaluation of Injector Location and Nozzle Design in a Direct-Injection Hydrogen Research Engine, *SAE Technical Paper* 2008-01-1785, 2008.
- [15] Rosati M., and Aleiferis, P.G., Hydrogen SI and HCCI Combustion in a Direct-Injection Optical Engine, *SAE Int. J. Engines*, 2009, pp. 1710–1736.
- [16] Scarcelli R., Wallner T., Salazar V., and Kaiser S., Modeling and Experiments on Mixture Formation in a Hydrogen Direct-Injection Research Engine, *SAE Int. J. Engines*, 2010, pp. 530–541.
- [17] Salazar V., and Kaiser S., An Optical Study of Mixture Preparation in a Hydrogen-fueled Engine with Direct Injection Using Different Nozzle Designs, *SAE Int. J. Engines* 2010, 119–131.
- [18] Scarcelli R., Wallner T., Matthias N., Salazar V. et al., Mixture Formation in Direct Injection Hydrogen Engines: CFD and Optical Analysis of Single- and Multi-Hole Nozzles, *SAE Int. J. Engines*, 2011, pp. 2361–2375.

- [19] Roy M., Kawahara N., Tomita E., and Fujitani T., High-Pressure Hydrogen Jet and Combustion Characteristics in a Direct-Injection Hydrogen Engine, *SAE Int. J. Fuels Lubr.*, 2012, pp. 1414–1425.
- [20] Nakagawa K., Yamane K., and Ohira T., Potential of Large Output Power, High Thermal Efficiency, Near-zero NO_x Emission, Supercharged, Lean-burn, Hydrogen-fuelled, Direct Injection Engines, *Energy Procedia*, Vol.29, 2012, pp. 455–462.
- [21] Aleiferis P.G., and Rosati M.F., Controlled autoignition of hydrogen in a direct-injection optical engine, *Combustion and Flame*, Vol.159, 2012, pp. 2500–2515.
- [22] Hamzehloo A., and Aleiferis, P.G., Computational Study of Hydrogen Direct Injection for Internal Combustion Engines, *SAE Technical Paper* 2013-01-2524, 2013.
- [23] Crist S., Sherman P.M., and Glass D.R., Study of the highly underexpanded sonic jet, *AIAA J.*, Vol.4, 1966, pp. 68–71.
- [24] Abbett M., The Mach Disk in Underexpanded Exhaust Plumes, *AIAA Journal*, Vol.9, 1971, pp. 512–514.
- [25] Donaldson C.DuP., and Snedeker R.S., A study of free jet impingement. Part 1. Mean properties of free and impinging jets. *J. Fluid Mech*, 1971, Vol.45, pp. 281–319.
- [26] Chuech S.G., Lai M.C., and Faeth G.M., Structure of turbulent sonic underexpanded free jets, *AIAA J.*, Vol.27, 1989, pp. 549–556.
- [27] Panda J., and Seasholtz R.G., Measurement of shock structure and shock–vortex interaction in underexpanded jets using Rayleigh scattering, *Phys. Fluids*, Vol.11, 1999.
- [28] White T., Milton B., 2008. Shock wave calibration of under expanded natural gas fuel jets, *Shock Waves*, Vol.18, 2008, pp. 353–364.
- [29] Inman A.J., Danehy P.M., Nowak R.J., and David W.A., Fluorescence Imaging Study of Impinging Underexpanded Jets, 46th AIAA Aerospace Sciences Meeting and Exhibit, 2008, Reno, Nevada, USA, AIAA Paper 2008-619.
- [30] Munday D., Gutmark E., Liu J., and Kailasanath K., Flow structure and acoustics of supersonic jets from conical convergent-divergent nozzles, *Phys. Fluids*, Vol. 23, 2011, 116102.
- [31] Yu J., Vuorinen V., Hillamo H., Sarjovaara T. et al., An Experimental Study on High Pressure Pulsed Jets for DI Gas Engine Using Planar Laser-Induced Fluorescence, *SAE Technical Paper* 2012-01-1655, 2012.
- [32] Yu J., Vuorinen V., Kaario O., Sarjovaara T., and Larmi M., Visualization and analysis of the characteristics of transitional underexpanded jets, *International Journal of Heat and Fluid Flow*, Vol.44, 2013, pp. 140–154.
- [33] Suzuki H., Endo M., and Sakakibara Y., Structure and Oscillation of Underexpanded Jet, *Open Journal of Fluid Dynamics*, Vol.3, 2013, pp. 85–91.
- [34] Irie T., Yasunobu T., Kashimura H., and Setoguchi T., Characteristics of the Mack Disk in the underexpanded jet in which the back pressure continuously changes with time, *Journal of Thermal Science*, Vol.12, 2003, pp. 132–137.
- [35] Dauplain A., Cuenot B., and Gicquel Y.M., Large-eddy simulation of a stable supersonic jet impinging on flat plate, *AIAA J.* Vol.48, 2010, pp. 2325–2337.
- [36] Dubs P., Khalij M., Benelmir R., and Tazibt A., Study on the dynamical characteristics of a supersonic high pressure ratio underexpanded impinging ideal gas jet through numerical simulations, *Mechanics Research Communications*, Vol.38, 2011, pp. 267–273.
- [37] Vuorinen V., Yu J., Tirunagari S., Kaario O., Larmi M., et al, Large-eddy simulation of highly underexpanded transient gas jets, *Phys. Fluids*, Vol.25, 2013, 016101.
- [38] Velikorodny A., and Kudriakov S., Numerical study of the near-field of highly underexpanded turbulent gas jets, *International Journal of Hydrogen Energy*, Vol.37, 2012, pp. 17390–17399.
- [39] Chin C., Li M., Harkin C., Rochwerger T., Chan L., and Ooi A., Investigation of the Flow Structures in Supersonic Free and Impinging Jet Flows, *Journal of Fluids Engineering*, Vol.135, 2013, 031202.
- [40] Ruggles A.J., and Ekoto I.W., Ignitability and mixing of underexpanded hydrogen jets, *International Journal of Hydrogen Energy*, Vol.37, 2012, pp. 17549–17560.
- [41] Gorré C., and Gamba M., Ham F., Investigation of an underexpanded hydrogen jet in quiescent air using numerical simulations and experiments, *Center for Turbulence Research, Stanford University*, Annual Research Briefs 2010, pp. 249–262.
- [42] Gorré C., and Iaccarino G., Large eddy and Reynolds-Averaged Navier-Stokes simulations of an underexpanded sonic jet, *7th European Symposium on Aerothermodynamics*, European Space Agency, Netherlands, 2011.
- [43] Khaksarfard R., Kameshki M.R., and Paraschivoiu M., Numerical simulation of high pressure release and dispersion of hydrogen into air with real gas model, *Shock Waves*, Vol.20, 2010, pp. 205–216.
- [44] Bonelli F., Viggiano A., and Magi V., A Numerical Analysis of Hydrogen Underexpanded Jets under Real Gas Assumption, *Journal of Fluids Engineering*, Vol.135, 2013, 121101.
- [45] Weiss J.M., and Smith W.A., Preconditioning Applied to Variable and Constant Density Flows, *AIAA J.*, Vol.33, 1995, pp. 2050–2057.
- [46] Weiss J.M., Maruszewski J.P., and Smith W. A., Implicit Solution of Preconditioned Navier–Stokes Equations Using Algebraic Multigrid, *AIAA J.*, Vol.37, 1999, pp. 29–36.
- [47] Liou M.S., and Steffen C.J., A New Flux Splitting Scheme, *Journal of Computational Physics*, Vol.107, 1993, pp. 23–39.
- [48] Chima R.V., and Liou M.S., Comparison of the AUSM⁺ and H-CUSP Schemes for Turbomachinery Applications, *AIAA Paper* 2003-4120. Also *NASA TM-2003-212457*.
- [49] Nicoud F., and Ducros F., Subgrid-Scale Stress Modelling Based on the Square of the Velocity Gradient Tensor, *Flow, Turbulence and Combustion*, Vol.62, 1999, pp. 183–200.
- [50] Cussler E.L., Diffusion: mass transfer in fluid systems, Third Edition, Cambridge University Press, 2009.
- [51] Owston R., Magi V., and Abraham J., Fuel-Air Mixing Characteristics of DI Hydrogen Jets, *SAE Int. J. Engines*, 2009, pp. 693–712.
- [52] Zhu Y., and Jiang P., Experimental and numerical investigation of the effect of shock wave characteristics on the ejector performance, *International Journal of Refrigeration*, Vol.40, 2014, pp. 31–42.